

Interface energies of $(100)_{\text{YSZ}}$ and $(111)_{\text{YSZ}}$ epitaxial islands on $(0001)_{\alpha\text{-Al}_2\text{O}_3}$ substrates from first principles

F. Lallet,^{1,*} N. Olivi-Tran,^{1,†} and Laurent J. Lewis^{2,‡}

¹*Laboratoire de Sciences des Procédés Céramiques et Traitements de Surface,
UMR-CNRS 6638, Ecole Nationale Supérieure de Céramiques Industrielles,
47 avenue Albert Thomas, 87065 Limoges cedex, France*

²*Département de Physique et Regroupement
Québécois sur les Matériaux de Pointe (RQMP),
Université de Montréal, C.P. 6128, Succursale Centre-Ville,
Montréal, Québec, Canada H3C 3J7*

(Dated: February 9, 2022)

Abstract

We present an *ab initio* study of the interface energies of cubic yttria-stabilized zirconia (YSZ) epitaxial layers on a $(0001)_{\alpha\text{-Al}_2\text{O}_3}$ substrate. The interfaces are modelled using a supercell geometry and the calculations are carried out in the framework of density-functional theory (DFT) and the local-density approximation (LDA) using the projector-augmented-wave (PAW) pseudopotential approach. Our calculations clearly demonstrate that the $(111)_{\text{YSZ}}|| (0001)_{\alpha\text{-Al}_2\text{O}_3}$ interface energy is lower than that of $(100)_{\text{YSZ}}|| (0001)_{\alpha\text{-Al}_2\text{O}_3}$. This result is central to understanding the behaviour of YSZ thin solid film islanding on $(0001)_{\alpha\text{-Al}_2\text{O}_3}$ substrates, either flat or in presence of defects.

PACS numbers: 68.35.bt, 68.55.aj

I. INTRODUCTION

Over the last few years, many experimental efforts have been expended on the fabrication of self-patterned, epitaxial nanocrystals (metallic, semiconductor or oxyde) on crystalline substrates.^{1,2,3,4,5,6} The aim is to synthesize homogeneous patterns of epitaxial crystals in order to induce quantum confinement — intimately related to the shape and the size of the nanocrystals — in order to achieve enhanced optical and/or magnetic properties.^{7,8,9,10,11,12,13} Several theoretical investigations have been concerned with the physical parameters responsible for the geometric properties of the nanocrystals.^{14,15,16,17,18,19}

The fabrication of such systems can be realised through various techniques involving the formation of nanometer-scale islands in a collective way, a process known as self-organisation. The basic idea is to promote the formation of nanocrystals on a crystalline substrate using thin solid films which demonstrate spontaneous evolution from a continuous 2D solid layer to a rough and/or discontinuous film, i.e., 3D epitaxial nanocrystals. The formation of the nanocrystals takes place during or after the deposition of the film as a way of reducing the total energy of the epitaxial {layer||substrate} system by the relaxation of the interface and/or surface stresses and strains. We briefly describe, in what follows, three of the most popular “bottom-up” approaches involved in epitaxial nanocrystals self-organisation processes.

A first approach is chemical vapor deposition (CVD), which consists in mixing chemical species in vacuum, which then react or decompose on the surface of a substrate to form a thin solid film. A second approach is physical vapor deposition (PVD), whereby matter is extracted from a solid target with, for example, a laser or an ion beam; the extracted ions attach to the surface of a substrate and eventually constitute a thin solid film. CVD and PVD, which lead to the formation of nanocrystals during the deposition process, have been successfully applied to the fabrication of self-organized arrays of semiconductor or metal nanocrystals, commonly called quantum dots (QDs). One of the most widely studied system is {Si||Ge}; this is characterized by the formation of epitaxial, faceted Ge QDs either at the top of a continuous Ge wetting layer (Stranski-Krastanov growth), or directly at the surface of the Si substrate (Volmer-Weber growth).^{20,21,22,23,24,25,26,27} A third approach goes by the deposition of a continuous thin xerogel film at the surface of a substrate by sol-gel dip-coating.²⁸ Through thermal treatment, the continuous thin solid film crystallizes

and breaks into several crystals through surface diffusion,^{29,30,31} leading to the formation of discrete epitaxial islands on the surface of the substrate. In this case, unlike PVD or CVD, the formation of the epitaxial islands takes place after the deposition of the film. This technology is particularly efficient for designing arrays of oxide nano-islands, as recently demonstrated by Bachelet.³²

In this article, we are concerned with the $\{\text{YSZ}||(\text{0001})_{\alpha\text{-Al}_2\text{O}_3}\}$ system, where epitaxial nano-islands of cubic yttria-stabilized zirconia (YSZ) form during the thermal treatment of a thin xerogel film deposited by sol-gel dip-coating on a $(\text{0001})_{\alpha\text{-Al}_2\text{O}_3}$ substrate. Experimentally, Bachelet *et al.* have demonstrated that the shape and size of the YSZ islands are directly linked to their epitaxial relation with the substrate.³² Indeed, for a substrate without defects, the islands are top-flat with large interface areas and exhibit the following in-plane and out-of-plane crystallographic orientations:

$$(\text{100})_{\text{YSZ}}||(\text{0001})_{\alpha\text{-Al}_2\text{O}_3}, \quad [\text{001}]_{\text{YSZ}}||[\text{010}]_{\alpha\text{-Al}_2\text{O}_3}, \quad (1)$$

$$(\text{100})_{\text{YSZ}}||(\text{0001})_{\alpha\text{-Al}_2\text{O}_3}, \quad [\text{001}]_{\text{YSZ}}||[\text{110}]_{\alpha\text{-Al}_2\text{O}_3}, \quad (2)$$

whereas for a substrate containing defects, some islands are round and thicker than the top-flat ones but with lower interface areas, and possess the in-plane and-out-of plane orientations:

$$(\text{111})_{\text{YSZ}}||(\text{0001})_{\alpha\text{-Al}_2\text{O}_3}, \quad [\text{1}\bar{1}0]_{\text{YSZ}}||[\text{110}]_{\alpha\text{-Al}_2\text{O}_3}. \quad (3)$$

The morphological evolution of the thin solid film into discrete nano-islands proceeds by an abnormal grain growth driven by the interface during thermal treatment.³³ From our previous theoretical investigations of this system,³¹ and in good agreement with experimental results, we demonstrated that the shape and size transition from top-flat to round is linked to the presence of defects at the surface of the substrate which induce enhanced growth in height.

However, the preferred formation of interfaces (1) and (2) over interface (3) for a perfect $(\text{0001})_{\alpha\text{-Al}_2\text{O}_3}$ substrate is not clearly understood. On the basis of energy considerations it can be argued that, to first order, an epitaxial crystal is in equilibrium with both the vacuum through the free surface energy and with the substrate through the interface energy, where both energies are related to the crystallographic orientations. Using *ab initio* methods, Ballabio *et al.* have demonstrated that the free surface energy of $(\text{100})_{\text{YSZ}}$ is higher than that of $(\text{111})_{\text{YSZ}}$.³⁴

In this article, we propose to examine the interface energies defined by the epitaxial relations (1), (2), and (3) on a perfect $(0001)_{\alpha-\text{Al}_2\text{O}_3}$ substrate. We argue that the knowledge of the interface energies is sufficient for a proper comparison of the behaviour of the three interfaces. There are several theoretical investigations of $\{\text{metal}||\text{oxide}\}$ interfaces, in particular for $(0001)_{\alpha-\text{Al}_2\text{O}_3}$ because of its technological significance in thermal barrier coatings and catalytic devices.^{35,36,37,38,39,40,41,42} However, few studies have been devoted to $\{\text{oxide}||\text{oxide}\}$ interfaces⁴³ and, to the best of our knowledge, none have been concerned with the $\{\text{YSZ}||(\text{0001})_{\alpha-\text{Al}_2\text{O}_3}\}$ system. Our calculations clearly demonstrate that interface (3) is energetically favored over interfaces (1) and (2). We therefore propose a general explanation for the behaviour of the islanding process of YSZ thin solid films on $(0001)_{\alpha-\text{Al}_2\text{O}_3}$ substrates, either perfect or with surface defects, in the light of experimental and theoretical investigations.^{31,32}

The article is constructed as follows. In section II we give the details of the numerical procedure, followed in section III by a demonstration of the ability of the PAW pseudopotentials to reproduce the correct structural properties of α and κ - Al_2O_3 , the low-pressure polymorphs of ZrO_2 , and the Y_2O_3 bixbyite structure. In section IV we first discuss the calculation of the unrelaxed and relaxed stoichiometric free surface energies, then we present the atomic-scale models for the the (1), (2) and (3) $\{\text{YSZ}||(\text{0001})_{\alpha-\text{Al}_2\text{O}_3}\}$ interfaces and the results of our calculations. A general conclusion is provided in Section V.

II. COMPUTATIONAL DETAILS

All calculations were carried out in the framework of density functional theory (DFT) using the *Abinit* code,⁴⁴ where the wave functions are expanded in plane waves. The atomic pseudopotentials were constructed with the *atompaw* program⁴⁵ within the frozen-core approximation, using the projector-augmented-waves (PAW) method originally proposed by Blöchl.⁴⁶ For the exchange-correlation functional, we employed the local density approximation (LDA) as parametrized by Perdew and Wang.⁴⁷ The atomic wave functions were augmented with 3, 6, 5, and 5 projectors within a spherical augmentation region of radii 1.4, 1.8, 2, and 2 Bohrs for O, Al, Y, and Zr atoms, respectively. The 2s and 3s semi-core states of Al, as well as the 4s and 4p semi-core states of Y and Zr, were treated as valence states to generate the pseudo-wave and projector functions within the augmentation

region. We found that taking Y and Zr semi-core states as valence is debatable. Indeed, Jansen⁴⁸ demonstrated that, due to the large energy difference between O and Zr($4s, 4p$) resonances, the O-Zr($4s, 4p$) hybridization is weak in ZrO_2 . This argument was applied by Christensen and Carter to study the free surfaces of ZrO_2 low-pressure polymorphs⁴⁹ and the $\{(001)_{\text{ZrO}_2} || (10\bar{1}2)_{\alpha-\text{Al}_2\text{O}_3}\}$ interface.⁴³ However, in previous studies of bulk YSZ by Stapper *et al.*⁵⁰ and of YSZ slabs by Ballabio *et al.*,³⁴ the ($4s, 4p$) semi-core states of Y and Zr were treated as valence. Here, we are also dealing with YSZ bulk and slab structures, as it is our purpose to characterize the $\{\text{YSZ} || (0001)_{\alpha-\text{Al}_2\text{O}_3}\}$ interfaces. In section III we will demonstrate that the treatment of $4s$ and $4p$ semi-core states of Y and Zr as valence states is appropriate to accurately describe the structural properties of Y_2O_3 bixbyite and ZrO_2 low-pressure polymorphs.

Additional details are as follows. For the α and κ phases of Al_2O_3 , as well as the ZrO_2 low-pressure polymorphs and the Y_2O_3 bixbyite structure, all discussed in section III, we used a kinetic energy cutoff of 15 Ha (≈ 408 eV) and $2 \times 2 \times 2$ Monkhorst-Pack grid⁵¹ for the Brillouin-zone integrations of bulk unit cells, which is a standard choice for wide band gap oxides.⁴³ With these parameters, the total energies are converged to within 10^{-2} Ha/atom (0.2 eV/atom) and the forces to better than 10^{-4} Ha/(Bohr. atom). The atoms were relaxed to their ground-state positions using the Broyden-Fletcher-Goldfarb-Shanno (BFGS) algorithm.⁵²

The slab geometry for the $(0001)_{\alpha-\text{Al}_2\text{O}_3}$ system is described in section IV; in this case we used a $2 \times 2 \times 1$ Monkhorst-Pack grid in the z direction. For the (1), (2) and (3) $\{\text{YSZ} || (0001)_{\alpha-\text{Al}_2\text{O}_3}\}$ interfaces, and according to previous studies,^{34,50} only the Γ point was used to integrate the Brillouin zone. The convergence criteria for relaxation were the same as above.

III. STRUCTURAL PARAMETERS OF THE BULK PHASES

We present here our results for the various bulk phases in order to ensure that our approach yields the correct structural parameters. For this purpose, we computed the relaxed lattice parameters and ionic positions (we follow the Wyckoff convention⁵³) for each crystalline structure. We also computed the ground state energies E as a function of the volume

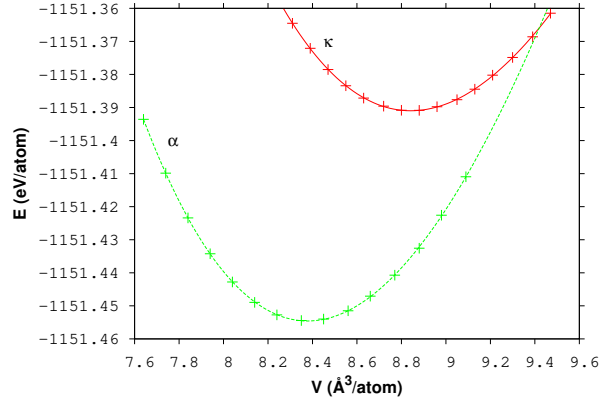


FIG. 1: (Color online) Energy vs volume for α -Al₂O₃ and κ -Al₂O₃, as indicated

V of the unit cell; these can be fitted to the Murnaghan equation of state:⁵⁴

$$E(V) = E_0 + \left(\frac{B_0 V}{B'_0} \right) \left(\frac{(V_0/V)^{B'_0}}{B'_0 - 1} + 1 \right) - \frac{B_0 V_0}{B'_0 - 1} \quad (4)$$

with

$$B'_0 = \left(\frac{dB_0}{dP} \right)_{(P=0)}, \quad (5)$$

thus yielding the equilibrium volume V_0 and the bulk modulus B_0 ; P is the pressure.

α -Al₂O₃ (also known as corundum) is the thermodynamically stable polymorph of alumina at low pressure. It is widely used for epitaxial thin solid film growth, in particular the (0001) “C-cut” and (10 $\bar{1}2$) “R-cut” families of planes. It has space group $R\bar{3}c$ and can be represented either by a rhombohedral unit cell with 10 atoms (2 Al₂O₃ molecular units) or a hexagonal cell with 30 atoms (6 Al₂O₃ molecular units). In our calculations, we assigned the initial positions of the Al and O ions according to the (experimental) values of Wyckoff.⁵³ In the conventional hexagonal cell, there are 6 oxygen planes organised in the ...ABABAB... closed-packed stacking sequence in the c direction, with the aluminum ions occupying 2/3 of the octahedral sites.

Apart from the α phase, there are two metastable polymorphs of alumina which are of practical interest, viz. κ -Al₂O₃ and γ -Al₂O₃; we focus on κ -Al₂O₃ hereafter. This polymorph can be synthesized by CVD and, because of its hardness, is used as surface coating.⁵⁵ The crystalline structure of κ -Al₂O₃ is orthorhombic, space group $Pna2_1$, with 40 atoms (8 Al₂O₃ molecular units) in the unit cell.⁵⁶ There are four oxygen planes in the cell, organized in the ...ABCABCABC... stacking sequence, and the aluminum ions fill the tetrahedral

TABLE I: Parameters of the Murnaghan equation of state, V_0 ($\text{\AA}^3/\text{atom}$), B_0 (GPa), and B'_0 , for $\alpha\text{-Al}_2\text{O}_3$ and $\kappa\text{-Al}_2\text{O}_3$, and comparison with other results from the literature.

	$\alpha\text{-Al}_2\text{O}_3$			$\kappa\text{-Al}_2\text{O}_3$		
	V_0	B_0	B'_0	V_0	B_0	B'_0
LDA ^a	8.38	260	4	8.84	239	4.3
LDA ^b		239				
LDA ^c	8.51	244	4.305			
LDA ^d	8.36	257	4.05			
Exp. ^e	8.53	254.4	4.275			
Emp. ^f				8.802	229.2	
LDA ^g				8.754	251.8	

^aThis work

^bRef. 39

^cRef. 62

^dRef. 63

^eRef. 64

^fRef. 58; ‘Emp.’ stands for ‘empirical model’

^gRef. 60

and/or octahedral sites.⁵⁷ The positions of the Al atoms in this structure is under debate. Indeed, Belonoshko *et al.*⁵⁸ proposed a model in which 2/3 of the octahedral sites are filled with Al ions as in $\alpha\text{-Al}_2\text{O}_3$ whereas, according to the theoretical studies of Yourdshahyan *et al.*, the most stable structure is one of the nine possible configurations for which the Al are only in octahedral positions.^{59,60} In this work, for the sake of simplicity and clarity, we have chosen to fix the reduced coordinates of Al and O ions to the experimental values issued from the Rietveld refinement of Smrcok and al.,⁶¹ thus, all the ions are in position 4a with coordinates (x_1, y_1, z_1) for Al and (x_2, y_2, z_2) for O, with symmetry operations $(x, y, z; -x, -y, z + 1/2; x + 1/2, -y + 1/2, z; -x + 1/2, y + 1/2, z + 1/2)$.

The $E(V)$ curves for both polymorphs are presented in Fig. 1 and the parameters of the Murnaghan equation of state are provided in Table I. One can see that our *ab initio* calculations do reproduce the correct relative stability of the two phases; it is indeed known that at low pressure the $\kappa\text{-Al}_2\text{O}_3 \rightarrow \alpha\text{-Al}_2\text{O}_3$ phase transition occurs around 1000°C.

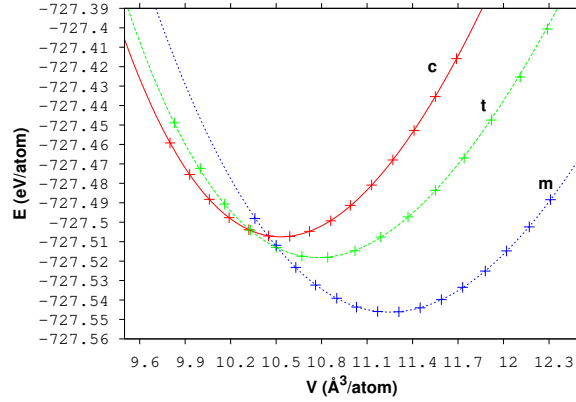


FIG. 2: (Color online) Energy vs volume for the low-pressure polymorphs of ZrO_2 , as indicated

The lattice parameters of the rhombohedral and hexagonal phases of $\alpha\text{-Al}_2\text{O}_3$ are summarized in Table II. The parameters for the hexagonal cell, \vec{a}_{h1} , \vec{a}_{h2} , and \vec{c}_h , are deduced from the rhombohedral ones, \vec{a}_{rh1} , \vec{a}_{rh2} , and \vec{a}_{rh3} , as follows:⁶⁵

$$\vec{a}_{h1} = \vec{a}_{rh1} - \vec{a}_{rh2} \quad (6)$$

$$\vec{a}_{h2} = \vec{a}_{rh2} - \vec{a}_{rh3} \quad (7)$$

$$\vec{c}_h = \vec{a}_{rh1} + \vec{a}_{rh2} + \vec{a}_{rh3} \quad (8)$$

with $a_{rh} = \|\vec{a}_{rh1}\| = \|\vec{a}_{rh2}\| = \|\vec{a}_{rh3}\|$, $a_h = \|\vec{a}_{h1}\| = \|\vec{a}_{h2}\|$, and $c_h = \|\vec{c}_h\|$. The parameters for (orthorhombic) $\kappa\text{-Al}_2\text{O}_3$ are a_0 , b_0 and c_0 .

We now turn to zirconium dioxide, an important material for applications in optical, mechanical and thermal coatings. Here we are concerned with the low-pressure polymorphs of ZrO_2 stoichiometry. From 0 to 1400 K, ZrO_2 is monoclinic ('m'; this phase is called baddeleyite), of space group $P2_1/c$;⁶⁸ between 1400 and 2650 K, it is tetragonal ('t'), of space group $P4_2/nmc$;⁶⁹ finally, above 2650 K and all the way to the melting point, it is cubic ('c'), of space group $Fm\bar{3}m$.⁷⁰ Here we describe the three phases through their conventional unit cells with 12 atoms (4 ZrO_2 molecular units). Table III presents the parameters of the Murnaghan equation of state derived from the $E(V)$ curves of Fig. 2. Our calculations reproduce the correct relative stability of the three polymorphs and our fitted parameters agree with previous theoretical and experimental results. The structural parameters are provided in Table IV.

Finally, we discuss the structural parameters of Y_2O_3 (bixbyite), which is body-centered cubic, space group $Ia\bar{3}$. This can be viewed in the conventional unit cell with 80 atoms

TABLE II: Lattice parameters for α -Al₂O₃ in the rhombohedral and hexagonal cells, and for κ -Al₂O₃ in the orthorhombic cell (Å), and comparison with other results from the literature; α_{rh} is the angle of the rhombohedral cell (degrees).

	α -Al ₂ O ₃				κ -Al ₂ O ₃		
	a_{rh}	α_{rh}	a_h	c_h	a_0	b_0/a_0	c_0/a_0
LDA ^a	5.114	54.952	4.717	12.987	4.836	1.711	1.835
LDA ^b			4.714	12.861			
LDA ^c			4.767	12.969			
Emp. ^d			4.773	12.990			
Exp. ^e			4.7589	12.991			
Exp. ^f			4.760	12.993			
Exp. ^g	5.128	55.333	4.7628	13.0032			
Emp. ^h					4.770	1.731	1.874
LDA ⁱ					4.804	1.7137	1.8435
Exp. ^j					4.8340	1.719	1.8480
Exp. ^k					4.69	1.744	1.891

^aThis work

^bRef. 39

^cRef. 62

^dRef. 66

^eRef. 65

^fRef. 67

^gRef. 53

^hRef. 58

ⁱRef. 60

^jRef. 61

^kRef. 56

and lattice parameter $a = 10.604$ Å,⁵³ or in the primitive unit cell with 40 atoms and lattice parameter $a' = a\sqrt{3}/2$. In this work, we have used the primitive unit cell; there are two nonequivalent yttrium sites, $8a$ for Y_I of coordinates (1/4, 1/4, 1/4) and $24d$ for Y_{II} of coordinates ($u, 0, 1/4$). The oxygen site is $48e$ of coordinates (x, y, z). The relevant symmetry operations can be found elsewhere.⁵³ Table V presents the parameters of the

TABLE III: Parameters of the Murnaghan equation of state, V_0 ($\text{\AA}^3/\text{atom}$), B_0 (GPa), and B'_0 , for m-, t-, and c-ZrO₂, and comparison with other results from the literature.

	LDA ^a			LDA ^b		
	m	t	c	m	t	c
V_0	11.25	10.78	10.53	11.68	11.13	10.91
B_0	203	225	273	185	197	268
B'_0	2.4	4.7	4.3	1.8	5.0	3.6
	Experiment					
	m	t	c			
V_0	11.74 ^c	11.64 ^d	10.86 ^e			
B_0	95-185 ^f	190-185 ^g	194-220 ^h 190 ⁱ			
B'_0	4-5 ^a					

^aThis work

^bRef. 50

^cRef. 70

^dRef. 69

^eRef. 53

^fRef. 71

^gRefs. 72, 73

^hRefs. 74, 75, 76

ⁱRef. 77

Murnaghan equation of state, the lattice parameter, and the internal ionic positions for Y_{II} and O.

The above results clearly establish the ability of the PAW method to reproduce the correct structural properties of the systems we are concerned with. In what follows, we present first the models used to simulate the (0001) surface of α -Al₂O₃ as well as the (100) and (111) surfaces of YSZ. We then discuss the method for constructing the interface supercells, which will be used to calculate the interface energies.

TABLE IV: Lattice parameters for m-, t-, and c-ZrO₂ (Å), and comparison with other results from the literature; β is the angle of the monoclinic phase (degrees) and d_z is the tetragonal distortion of O atoms in the \vec{c} direction of the tetragonal phase.

	m			
	a	b/a	c/a	β
LDA ^a	5.085	1.020	1.025	99.31
LSDA ^b	5.136	1.020	1.029	99.43
Exp. ^c	5.1505	1.0119	1.0317	99.230
	t			c
	a	c/a	d_z	a
LDA ^a	5.046	1.029	0.049	5.02
LSDA ^b	5.086	1.013	0.040	5.082
Exp. ^c	5.15	1.02	0.065	5.07

^aThis work

^bRef. 42

^cRefs. 70 for m, 69 for t, and 53 for c

IV. INTERFACE ENERGIES OF {YSZ|| $(0001)_{\alpha\text{-Al}_2\text{O}_3}$ } (1), (2) AND (3)

In order to calculate the interface energies, we constructed supercell models consisting of a $(0001)_{\alpha\text{-Al}_2\text{O}_3}$ slab for the substrate and a $(100)_{\text{YSZ}}$ or $(111)_{\text{YSZ}}$ slab for the epitaxial layer. The supercells are parallelepipeds, and the interface is taken to be perpendicular to the z direction. Before proceeding, however, we consider the free surfaces and compute their unrelaxed and relaxed energies. Periodic boundary conditions are used; for free surfaces, a vacuum region is inserted in the supercell. Thus, in all cases there are two interfaces, either between the two materials or between the surface of the material and the vacuum.

The thickness of the slab must be sufficient to yield converged results and yet remain computationally manageable. To this end, one may first define two structures — one for the bulk and one for the slab — having the same number of atomic layers N ; the slab has two free surfaces owing to the presence of a vacuum region (see above). The free surface energy is then defined as the excess energy of the slab [(hkl) indices] relative to the bulk divided

TABLE V: Lattice parameter a (Å), parameters of the Murnaghan equation of state, V_0 (Å³/atom), B_0 (GPa) and B'_0 , and Wyckoff coordinates of Y_{II} and O for the Y_2O_3 bixbyite structure, and comparison with other results from the literature.

	a	V_0	B_0	B'_0	Y_{II} $-u$	O (x, y, z)
LDA ^a	10.481	14.31	160	4.4	0.0326	(0.3904,0.1512,0.3798)
LDA ^b	10.483		143	3.9	0.0327	(0.3905,0.1518,0.3803)
Exp. ^c	10.604				0.0314	(0.3890,0.1500,0.3770)

^aThis work

^bRef. 50

^cRef. 53

TABLE VI: Free surface energies $\gamma_{(0001)}$ (J/m²) of the unrelaxed and relaxed α -Al₂O₃ models for $N = 9, 12, 15, 18$ atomic layers (i.e., $\Delta N = 3$ here).

N	Unrelaxed ^a	Relaxed ^a	Relaxed ^b
9	4.14	2.08	2.02
12	4.22	2.14	
15	4.26	2.12	2.12
18	4.26	2.12	
21			2.12
27			2.12

^aThis work

^bRef. 39

by the surface S of the slab:

$$\gamma_{hkl}(N) = \frac{E_{\text{slab}}(N) - \frac{N}{\Delta N} \Delta E_{\text{bulk}}(N)}{S} \quad (9)$$

$$\Delta E_{\text{bulk}}(N) = E_{\text{bulk}}(N) - E_{\text{bulk}}(N - \Delta N), \quad (10)$$

where ΔN is the difference in the number of layers between two different slab models. The convergence of γ_{hkl} can be studied as a function of N .

However, Boettger has shown that this approach is not very accurate,⁷⁸ as the convergence

of $\gamma_{hkl}(N)$ depends on the thickness of both the slab and the bulk, but also on $\Delta E_{\text{bulk}}(N)$. He proposed to use, instead:

$$\gamma_{hkl}(N) = \frac{E_{\text{slab}}(N) - \frac{N}{\Delta N} \Delta E_{\text{slab}}(N')}{S} \quad (11)$$

$$\Delta E_{\text{slab}}(N') = E_{\text{slab}}(N') - E_{\text{slab}}(N' - \Delta N) \quad (12)$$

where N' is the number of layers for which the value of ΔE_{slab} is sufficiently converged to ensure that the behaviour of γ_{hkl} is a function of N only. Thus, in this approach, the term $\Delta E_{\text{bulk}}(N)$ in Eq. 9 is replaced by $\Delta E_{\text{slab}}(N')$ in Eq. 11, thereby reducing the convergence study of γ_{hkl} to slab calculations. For the sake of comparison with previous *ab initio* results on this system,³⁹ we used the Boettger method here.

A. (0001) $_{\alpha\text{-Al}_2\text{O}_3}$ free surface energy

Several calculations of stoichiometric and non stoichiometric free surface energies of (0001) $_{\alpha\text{-Al}_2\text{O}_3}$ have been reported in the literature.^{66,79,80,81,82,83,84} Here we deal only with stoichiometric systems; this choice is not restrictive as it was demonstrated that the most stable (0001) surface of $\alpha\text{-Al}_2\text{O}_3$ is stoichiometric, Al-terminated, in a wide range of P_{O_2} .^{81,85} Further, previous *ab initio* calculations³⁹ have shown that a vacuum thickness of 10 Å is sufficient and this is the value we have used. We have nevertheless studied the convergence with regard to the thickness of the solid, viz. 9, 12, 15, and 18 atomic layers.

The results, presented in Table VI, are found to be in very good agreement with those of Siegel.³⁹ One may note the huge differences between the unrelaxed and relaxed energies — the absolute differences are ~ 2 J/m². This is a consequence of the inward relaxation of the atomic planes in the z direction. Table VII gives the average relaxation of the atomic planes relative to the original bulk spacing. As found in previous calculations, the inward relaxation of the Al atomic plane is close to 80% and leads to the formation of sp^2 -like atomic bonding at the free surface. The inward relaxation of the top Al plane is related to the increase of the electronic density, yielding a lower free surface energy. Our study demonstrates that 15 atomic layers are needed to model accurately the bulk structure, but the results are already quite reasonable for $N = 9$, offering a good compromise between accuracy and computational workload as we discuss in Sec. IV C.

TABLE VII: Average relaxation of the atomic planes in the [001] direction for α -Al₂O₃, expressed as a proportion of the initial bulk spacing for $N = 9, 12, 15, 18$ atomic layers.

N	LDA ^a				LDA ^b
	9	12	15	18	15
Al-O	-87	-84	-83	-83	-83
O-Al	5	5	5	5	3
Al-Al	-52	-44	-44	-46	-46
Al-O	23	20	18	19	19
O-Al	23	6	5	4	4

^aThis work

^bRef. 39

B. (100)_{YSZ} and (111)_{YSZ} free surface energies

We now consider the YSZ (100) and (111) free surface energies. We follow the approach proposed by Stapper *et al.*⁵⁰ and Ballabio *et al.*³⁴ to build the bulk and slab structures. YSZ is a solid solution of Y₂O₃ in ZrO₂, of space group $Fm\bar{3}m$ (as c-ZrO₂). Proper simulation of YSZ depends on two parameters: (i) The size of the simulation cell, which must be large enough to provide a good statistical representation of the proportion of Y atoms and O vacancies (V_O) for a given molar proportion of Y₂O₃. (ii) The ground state energy, which depends on the relative positions of Y ions and O vacancies, and which cannot be chosen at random: Stapper *et al.* have indeed shown that the most stable configuration is that for which the O vacancies are next-nearest neighbours to yttrium atoms.⁵⁰

Here, the doping level of Y₂O₃ is set to 10% molar, consistent with the experimental studies of Bachelet *et al.*³² For consistency and comparison with previous works, the positions of the Y ions and the O vacancies are chosen such that two V_O 's cannot be closer to one another than third nearest neighbour; two Y's can be nearest neighbours but a Y cannot be closer to a V_O than next nearest neighbour. The bulk cell of (100)_{YSZ} is made up of 4 (Zr,Y) and 5 (O, V_O) atomic layers in the [100] direction ($N = 9$), for a total of 93 atoms (26 Zr, 61 O, 6 Y; 3 V_O). The dimensions of the bulk cell are $\delta x = \delta y = \delta z = 2a_{\text{YSZ}}$, where the theoretical lattice parameter is derived from the experimental relation established by

TABLE VIII: Unrelaxed and relaxed stoichiometric free surface energies $\gamma_{(100)}$ and $\gamma_{(111)}$ for YSZ (J/m^2).

Unrelaxed		Relaxed	
$\gamma_{(100)}$	$\gamma_{(111)}$	$\gamma_{(100)}$	$\gamma_{(111)}$
2.79 ^a	1.30 ^a	1.71 ^a	1.17 ^a
		1.75 ^b	1.04 ^b

^aThis work

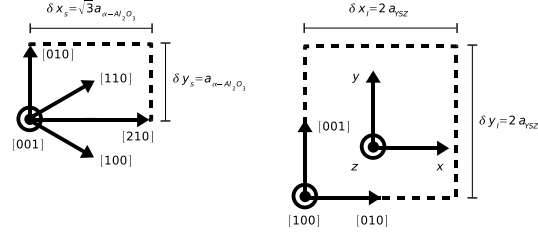
^bRef. 34

Pascual and Dúran,⁸⁶ $a_{\text{YSZ}} = a_0 + 0.003x$, with x the molar percent of Y_2O_3 . Using the values of a_0 given in Table IV and setting $x = 0.1$, we obtain $a_{\text{YSZ}} = 5.05 \text{ \AA}$. For the $(111)_{\text{YSZ}}$ cell, we have 3 (Zr,Y) and 6 (O, V_{O}) atomic layers in the $[111]$ direction ($N = 9$), for a total of 140 atoms (40 Zr, 92 O, 8 Y; 4 V_{O}). The dimensions of the cell are $\delta x = 2\sqrt{2}a_{\text{YSZ}}$, $\delta y = 2\sqrt{3/2}a_{\text{YSZ}}$, and $\delta z = \sqrt{3}a_{\text{YSZ}}$.

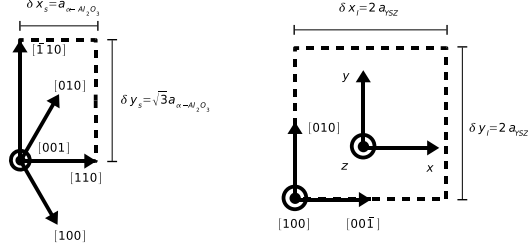
From these bulk cells, surface slabs are constructed by introducing a 10 \AA -thick vacuum layer along z . For consistency with the case of (Al-terminated) $\alpha\text{-Al}_2\text{O}_3$, we also consider stoichiometric surfaces hereafter so that, in both cases, the cells are terminated by an oxygen plane. In the case of $(100)_{\text{YSZ}}$, this requires half of the O atoms to be removed from each side of the slab. We placed one oxygen vacancy on each side of the slab cells on the free surfaces. The (100) and (111) free surface energies of YSZ, computed using Eq. 9, are presented in Table VIII; the areas of the free surfaces are $S = 8a_{\text{YSZ}}^2$ and $S = 8\sqrt{3}a_{\text{YSZ}}^2$, respectively.

We find good agreement with Ballabio *et al.* for the relaxed value of $\gamma_{(100)}$, but there is a small difference for $\gamma_{(111)}$; this might be due to the use of different relaxation schemes — BFGS here, vs Car-Parinello molecular dynamics⁸⁷ in Ref. 34. More important, however, we observe large changes arising from relaxation: $\sim 1.2 \text{ J/m}^2$ for $\gamma_{(100)}$ and $\sim 0.2 \text{ J/m}^2$ for $\gamma_{(111)}$, with an average inward relaxation of the top O plane of $\sim 25\%$ and $\sim 8\%$, respectively. These results are not surprising since (111) corresponds to a dense arrangement of the atomic planes, which is not the case for (100) .

Interface(1):



Interface(2):



Interface(3):

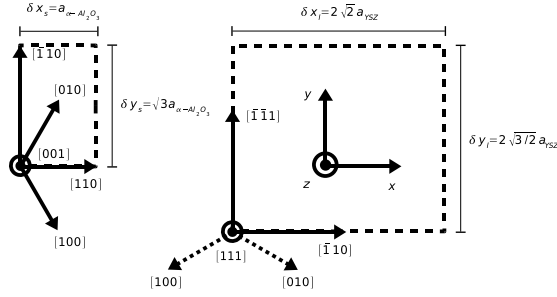


FIG. 3: Relative crystallographic orientations and dimensions of the $\alpha\text{-Al}_2\text{O}_3$ and YSZ unit cells (dashed lines) in the x and y directions for each interface model. For model (3), the YSZ $[100]$ and $[010]$ crystallographic orientations are out of the (x, y) plane and are represented as dotted lines.

C. $\{\text{YSZ}||(\text{0001})_{\alpha\text{-Al}_2\text{O}_3}\}$ interfaces

We now turn to the (1), (2), and (3) $\{\text{YSZ}||(\text{0001})_{\alpha\text{-Al}_2\text{O}_3}\}$ interface models, constructed from the structures discussed in the previous sections. More specifically, several unit cells must be assembled in the (x, y) plane so as to minimize the lattice mismatch; since the computational effort increases very rapidly with size, the number of cells of each material must be chosen such that the mismatch is no larger than a few percent in each supercell.

Figure 3 provides a schematic representation of the relative orientations of the two materials; ball-and-stick models are presented in Fig. 4. In practice, keeping the mismatch to within a few percent would require unit cells containing at least 500 atoms. This is clearly

TABLE IX: Lattice mismatches ϵ relative to the initial bulk spacings (%) and total number of atoms n_a for each interface model. N_{lx} and N_{sx} , and N_{ly} and N_{sy} , are the number of unit cells for the layer and the substrate in the x and y directions, respectively.

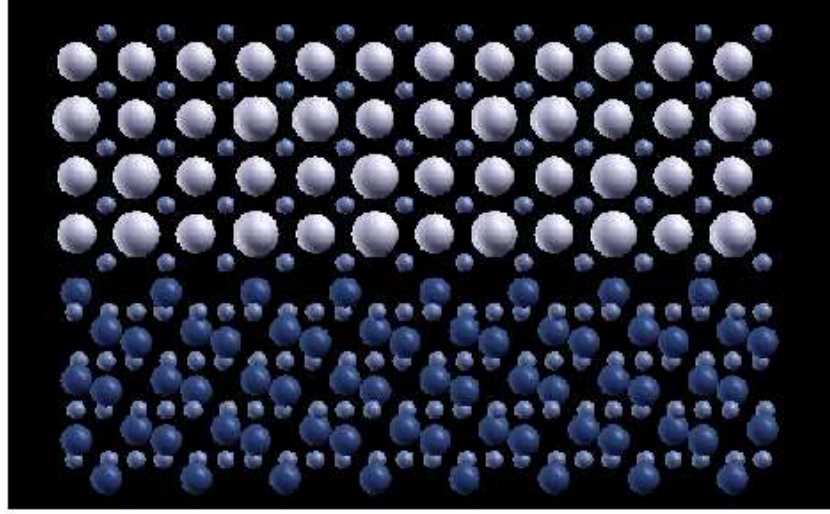
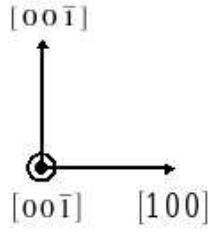
(1)	$N_{lx} = 3$	$N_{ly} = 1$	$n_a = 519$
	$N_{sx} = 4$	$N_{sy} = 2$	
	$\epsilon_{lx} = 3.93$	$\epsilon_{ly} = -3.30$	
	$\epsilon_{sx} = -3.64$	$\epsilon_{sy} = 3.53$	
(2)	$N_{lx} = 1$	$N_{ly} = 3$	$n_a = 519$
	$N_{sx} = 2$	$N_{sy} = 4$	
	$\epsilon_{lx} = -3.30$	$\epsilon_{ly} = 3.93$	
	$\epsilon_{sx} = 3.53$	$\epsilon_{sy} = -3.64$	
(3)	$N_{lx} = 1$	$N_{ly} = 2$	$n_a = 550$
	$N_{sx} = 3$	$N_{sy} = 3$	
	$\epsilon_{lx} = -0.45$	$\epsilon_{ly} = -0.46$	
	$\epsilon_{sx} = 0.46$	$\epsilon_{sy} = 0.47$	

unmanageable. In order to reduce the workload, we fixed the thickness of the α -Al₂O₃ substrate to 9 atomic layers; as mentioned earlier, while the system parameters are not fully converged at this value, they are nevertheless adequately described. In addition, as we will be comparing different structures with the same number of layers, systematic errors will cancel out to a large extent. The computational workload remains considerable, but was alleviated by running the calculations in parallel on up to 252 processors.

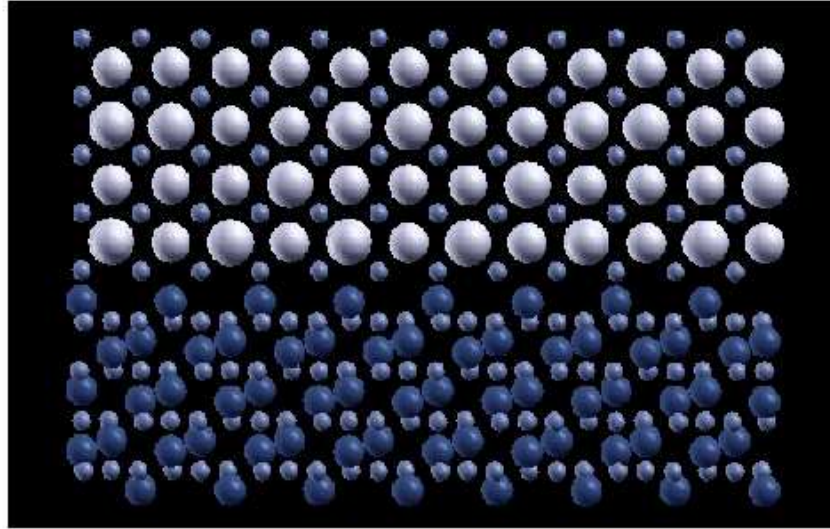
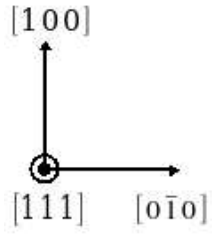
The details of the geometry of the three systems are given in Table IX: the mismatches are in all cases less than $\sim 4\%$. The distance between the substrate and the layer was fixed by assuming that the YSZ O plane at the interface lies at the position where an α -Al₂O₃ O plane would have been in an infinite system.

The total energy E_{int} of a given model structure can be related to the ideal work of

Interface(1):



Interface(2):



Interface(3):

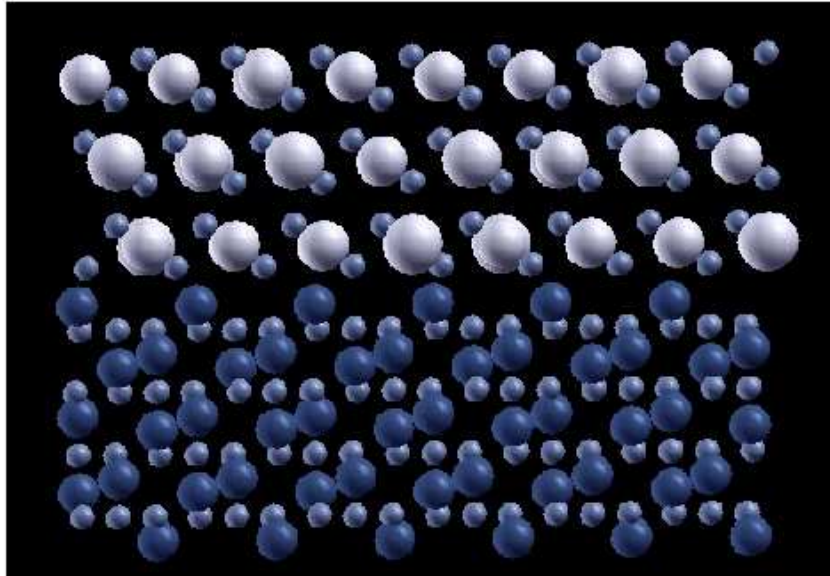
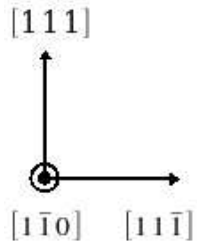


FIG. 4: (Color online) Side views of the unrelaxed interface models (1), (2) and (3). The Y and Zr atoms are white, the O atoms are light blue and the Al atoms are purple. The crystallographic orientations are those of the YSZ phase.

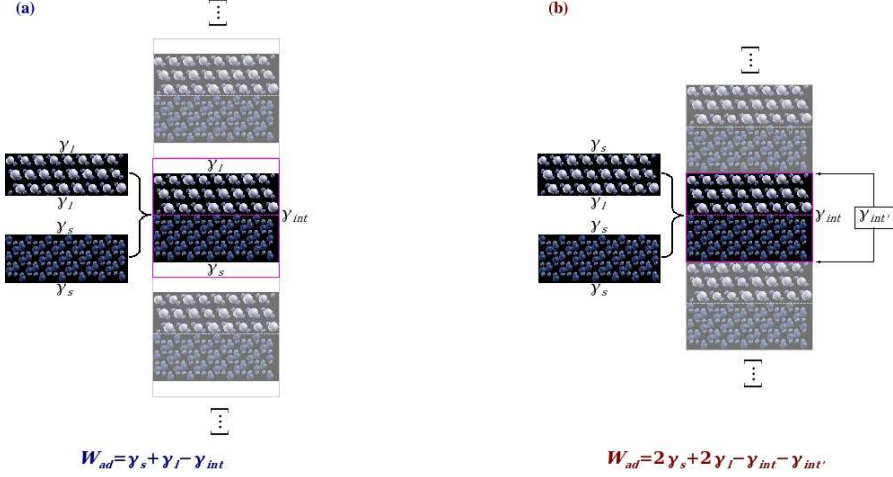


FIG. 5: (Color online) Schematic illustration of the geometry of the system and corresponding interface energies: periodically-replicated model interface structure (a) with vacuum and (b) without vacuum.

adhesion W_{ad} as follows:

$$W_{ad} = \frac{E_s + E_l - E_{int}}{S}, \quad (13)$$

where E_s and E_l are the total energies of the substrate and the layer, respectively, and S is the area of the interface. W_{ad} can be expressed in terms of the interface and surface energies as:

$$W_{ad} = 2\gamma_s + 2\gamma_l - \gamma_{int} - \gamma_{int'}, \quad (14)$$

where $\gamma_s = \gamma_{\alpha-\text{Al}_2\text{O}_3} = \gamma_{(0001)}$ and $\gamma_l = \gamma_{\text{YSZ}} = \gamma_{(100)}$ for interfaces (1) and (2) = $\gamma_{(111)}$ for interface (3). The quantity $\gamma_{int'}$ is the energy resulting from the presence of two interfaces in absence of vacuum. The significance of the various quantities entering Eqs. 13 and 14 in relation to the geometry of the models is schematically illustrated in Fig. 5.

One may argue that the interface energy between two solids is lower than the sum of the free energies of the two surfaces:

$$\gamma_{int'} \leq \gamma_{(0001)} + \gamma_{\text{YSZ}}. \quad (15)$$

Combining Eqs. 13, 14, and 15 yields a lower bound to the interface energy:

$$\gamma_{int} \geq \frac{E_{int} - (E_s + E_l)}{S} + \gamma_{(0001)} + \gamma_{\text{YSZ}}. \quad (16)$$

This is useful for comparing interface energies as γ_{YSZ} and $\gamma_{(0001)}$ are known. However, because the mismatches are finite (cf. Table IX), the substrate and layers are both under

TABLE X: Free surface energies for the strained, unrelaxed systems (J/m²).

	Interface (1)	Interface (2)	Interface (3)
	$\gamma_{(100)}$	$\gamma_{(100)}$	$\gamma_{(111)}$
	2.75	2.75	1.25
N	$\gamma_{(0001)}$	$\gamma_{(0001)}$	$\gamma_{(0001)}$
9	4.06	4.14	4.11
12	4.12	4.20	4.20
15	4.12	4.20	4.24
18	4.12	4.20	4.24

strain and, as a consequence, the values of E_s , E_l , γ_{YSZ} , and $\gamma_{(0001)}$ must reflect this. In practice, the values are adjusted for the actual lattice parameters of the substrate and the layers; the corresponding strained, unrelaxed free surface energies are listed in Table X.

One may note that for both layers and substrates, the strained unrelaxed free surface energies are strictly lower than their corresponding unstrained values (see Tables VI and VIII for comparison). This behaviour is related to both the evolution of the free surface (contraction or dilatation, see Table IX) and the modification of the electronic density. Using Eqs. 15 and 16, and the parameters listed in Table X, we have

$$4.48 \leq \gamma_{\text{int}(1)} \leq 6.81, \quad (17)$$

$$4.41 \leq \gamma_{\text{int}(2)} \leq 6.89, \quad (18)$$

$$2.46 \leq \gamma_{\text{int}(3)} \leq 5.36. \quad (19)$$

Our calculations demonstrate, therefore, that the interface energy for model (3) tends to be lower than that of models (1) and (2), implying that the former is the most thermodynamically stable of the three. This result is consistent with the continuity of the three-fold $\alpha - \text{Al}_2\text{O}_3$ (0001) symmetry axis with the YSZ (111) symmetry axis in model (3),³² i.e., electronic bonding is much stronger here than in models (1) and (2). As a consequence, on a perfect $\alpha - \text{Al}_2\text{O}_3$ substrate, the creation of a type-(3) interface requires much more energy than interfaces of types (1) and (2) because it is more strongly bonded. Thus, at the beginning of the islanding process, when the thin solid film still exhibits a large interface area with the substrate, the formation of interfaces (1) and (2) is favored over interface (3).

As a consequence, $(111)_{\text{YSZ}}$ islands are not expected to form on a perfect $\alpha - \text{Al}_2\text{O}_3$ substrate — only $(100)_{\text{YSZ}}$ islands with large interface areas should be observed.

On an imperfect substrate, now, the islands nucleating at the location of the defects are subject to enhanced growth in height.³¹ As a result, the interface area decreases and the energy cost required for the island to create interface (3) decreases with regard to the whole internal energy of the island. This allows one to understand why, on rough substrates, $(111)_{\text{YSZ}}$ rounded islands are observed only at the location of defects.

V. CONCLUSION

We have demonstrated using an *ab initio* approach that the $(111)_{\text{YSZ}}|| (0001)_{\alpha - \text{Al}_2\text{O}_3}$ interface is thermodynamically more stable than $(100)_{\text{YSZ}}|| (0001)_{\alpha - \text{Al}_2\text{O}_3}$. This result allows us to understand and coherently describe the islanding process during the thermal treatment of YSZ on $\alpha - \text{Al}_2\text{O}_3$, either perfect or with defects. On a perfect substrate, the formation of the $(100)_{\text{YSZ}}|| (0001)_{\alpha - \text{Al}_2\text{O}_3}$ interface is energetically favored over $(111)_{\text{YSZ}}|| (0001)_{\alpha - \text{Al}_2\text{O}_3}$, opening up the way to the formation of $(100)_{\text{YSZ}}$ islands on the perfect substrate. On an imperfect surface, the formation of islands at the location of defects leads to enhanced growth in height. As the interface area decreases, the energy cost required to form interface (3) does too. As a consequence, the $(111)_{\text{YSZ}}|| (0001)_{\alpha - \text{Al}_2\text{O}_3}$ interface can form at the location of defects, which explains that both $(100)_{\text{YSZ}}$ and $(111)_{\text{YSZ}}$ islands are observed in this case.

Acknowledgements

This work has been supported by grants from the Natural Sciences and Engineering Research Council of Canada (NSERC) and the *Fonds Québécois de la Recherche sur la Nature et les Technologies* (FQRNT). We are indebted to the *Réseau Québécois de Calcul de Haute Performance* (RQCHP) for generous allocations of computer resources. We are grateful to Michel Côté, Simon Pesant, Guillaume Dumont for help with the *Abinit* code, and Michel Béland for advice on code optimisation.

* Electronic address: flallet@ensci.fr

- [†] Electronic address: n'olivi-tran@ensci.fr
- [‡] Electronic address: Laurent.Lewis@UMontreal.CA
- ¹ V. Repain, J. M. Berroir, S. Rousset, and J. Lecoer, Surf. Sci. **447** L152 (2000).
 - ² F. Silly and M. R. Castell, Phys. Rev. Lett. **94** 046103 (2005).
 - ³ K. Alchalabi, D. Zimin, G. Kostorz, and H. Zogg, Phys. Rev. Lett. **90** 026104 (2003).
 - ⁴ J. C. Nie, H. Yamasaki, and Y. Mawatari Phys. Rev. B **70**, 195421 (2004).
 - ⁵ F. Sanchez, U. Lüders, G. Herranz, I. C. Infante, J. Fontcuberta, M. V. Garcia-Cuenca, C. Ferrater, and M. Varela, Nanotech. **16** S190 (2005).
 - ⁶ E. Vasco, S. Karthäuser, R. Dittman, J. Q. He, C.L. Jia, K. Szot, and R. Waser, Ad. Mater. **17** 281 (2005).
 - ⁷ Y. He, C. C. Zhu, and J. Zhang, Micro. J. **35** 389-392 (2004).
 - ⁸ W. Heiss, E. Kaufmann, M. Böberl, T. Schwarzl, G. Springholz, G. Hesser, F. Schäffler, K. Koike, H. Harada, M. Yano, *et al.*, Physica E **35** 241 (2006).
 - ⁹ D. Zhao, Y. Zhu, and J. Liu, Solid-State Elec. **50**, 268-271 (2006).
 - ¹⁰ J. Prokop, A. Kukunin, and H. J. Elmers, Phys. Rev. B **75** 144423 (2007).
 - ¹¹ V. Tasco, N. Deguffroy, A. N. Baranov, E. Tournié, B. Satpati, A. Trampert, M. Dunaevski, and A Titkov, J. Cryst. Growth **301** 713-717 (2007).
 - ¹² V. I. Klimov, S. A. Ivanov, J. Nanda, M. Achermann, I. Bezel, J. A. McGuire, and A. Piryatinski, Nature **447** 441 (2007).
 - ¹³ J. Wensch, L. Ebel, C. Gould, G. Schmidt, L. W. Molenkamp, and K. Brunner, J. Cryst. Growth **301-302** 638-641 (2007).
 - ¹⁴ L. Nurminen, A. Kuronen, and K. Kaski, Phys. Rev. B **63**, 035407 (2000).
 - ¹⁵ M. Kalke and D. V. Baxter, Surf. Sci. **477**, 95-101 (2001).
 - ¹⁶ P. Liu, Y. W. Zhang, and C. Lu, Phys. Rev. B **68**, 035402 (2003).
 - ¹⁷ T. Kawamura and T. Natori, Surf. Sci. **438**, 148-154 (1999).
 - ¹⁸ G. Russo and P. Smereka, J. Comp. Phy. **214**, 809-828 (2006).
 - ¹⁹ F. Lallet, A. Dager, and N. Olivi-Tran, Phys. Stat. Sol. C **4**, 1189-1192 (2006).
 - ²⁰ P. Sutter and M. G. Lagally, Phys. Rev. Lett. **84**, 4637 (2000).
 - ²¹ R. M. Tromp, F. M. Ross, and M. C. Reuter, Phys. Rev. Lett. **84**, 4641 (2000).
 - ²² G. Capellini, M. De Seta, and F. Evangelisti, Mater. Sci. Eng. B **89**, 184-187 (2001).
 - ²³ A. Portavoce, M. Kammler, R. Hull, M. C. Reuter, M. Copel, F. M. Ross, Phys. Rev. B **70**,

- 195306 (2004).
- ²⁴ P. S. Chen, Z. Pei, Y. H. Peng, S. W. Lee, and M. -J. Tsai, Mater. Sci. Eng. B **108**, 213-218 (2004).
 - ²⁵ R. J. Wagner and E. Gulari, Phys. Rev. B **69**, 195312 (2004).
 - ²⁶ R. J. Wagner and E. Gulari, Surf. Sci. **590**, 1-8 (2005).
 - ²⁷ B. Voigtländer, Surf. Sci. Rep. **43**, 127-254 (2001).
 - ²⁸ J. F. Brinker and G. W. Scherer, *Sol Gel Science: the physics and chemistry of sol gel processing* (Academic, New York, 1990).
 - ²⁹ N. Olivi-Tran, A. Boule, A. Gaudon, and A. Dauger, Phys. Lett. A **351**, 426-430 (2006).
 - ³⁰ X. Zhou, N. Olivi-Tran, A. Gaudon, and A. Dauger, J. of Alloys and Comp. **434-435**, 555-558 (2007).
 - ³¹ F. Lallet, R. Bachelet, A. Dauger, and N. Olivi-Tran, Phys. Rev. B **74**, 075411 (2006).
 - ³² R. Bachelet, A. Boule, B. Soulestin, F. Rossignol, A. Dauger, and R. Guinebretiere, Thin Solid Films **515**, 7080-7085 (2007).
 - ³³ F. F. Lange, Science **273**, 903 (1996).
 - ³⁴ G. Ballabio, M. Bernasconi, F. Pietrucci, and S. Serra, Phys. Rev. B **70**, 075417 (2004).
 - ³⁵ D. M. Duffy, J. H. Harding, and A. M. Stoneham, Acta Mater. **44**, 3293-3298 (1996).
 - ³⁶ W. Zhang, J. R. Smith, Phys. Rev. B **61**, 16883 (2000).
 - ³⁷ I. G. Batyrev, A. Alavi and M. W. Finnis, Phys. Rev. B **62**, 4698 (2000).
 - ³⁸ W. Zhang and J. R. Smith, Phys. Rev. Lett. **85**, 3225 (2000).
 - ³⁹ D. J. Siegel, L. G. Hector, and J. B. Adams, Phys. Rev. B **65**, 085415 (2002) and references therein.
 - ⁴⁰ S. B. Sinnott and E. C. Dickey, Mater. Sci. Eng. R **43**, 1-59 (2003) and references therein.
 - ⁴¹ S. V. Dmitriev, N. Yoshikawa, and Y. Kagawa, Comp. Mat. Sci. **29**, 95-102 (2004).
 - ⁴² A. Christensen and Emily A. Carter, J. Chem. Phys. **114**, 5816 (2001).
 - ⁴³ A. Christensen and Emily A. Carter, Phys. Rev. B **62**, 16968 (2000).
 - ⁴⁴ X. Gonze, J.-M. Beuken, R. Caracas, F. Detraux, M. Fuchs, G.-M. Rignanese, L. Sindic, M. Verstraete, G. Zerah, F. Jollet, M. Torrent, A. Roy, M. Mikami, Ph. Ghosez, J.-Y. Raty, and D.C. Allan, Comput. Mat. Sci. **25**, 478-492 (2002).
 - ⁴⁵ A.R. Tackett, N.A.W. Holzwarth, and G.E. Matthews, Comp. Phys. Com. **135** 329-347, 348-376 (2001).

- ⁴⁶ P. E. Blöchl, Phys. Rev. B **50**, 17953 (1994).
- ⁴⁷ J.P. Perdew and Y. Wang, Phys. Rev. B **45**, 13244 (1992).
- ⁴⁸ H. J. F. Jansen, Phys. Rev. B **43**, 7267 (1991).
- ⁴⁹ A. Christensen and Emily A. Carter, Phys. Rev. B **58**, 8050 (1998).
- ⁵⁰ G. Stapper, M. Bernasconi, N. Nicoloso, and M. Parrinello, Phys. Rev. B **59**, 797 (1999).
- ⁵¹ H.J. Monkhorst and J. D. Pack, Phys. Rev. B **13**, 5188 (1976).
- ⁵² C. Broyden, Math. Comput. **19**, 577 (1965).
- ⁵³ R. W. G. Wyckoff, *Crystal Structures*, 2nd ed. (Interscience Publishers, New York, 1963), Vols. 1 and 2.
- ⁵⁴ D. Murnaghan, Proc. Natl. Acad. Sci. USA **30**, 244 (1944).
- ⁵⁵ S. Ruppi, J. of Phys. IV **11**, 847-859 (2001).
- ⁵⁶ P. Liu and J. Skogsmo, Acta Cryst. B **47**, 425-433 (1991).
- ⁵⁷ B. Holm, R. Ahuja, Y. Yourdshahyan, B. Johansson, and B. I. Lundqvist, Phys. Rev. B **59**, 12777 (1999).
- ⁵⁸ A. B. Belonoshko, R. Ahuja, and B. Johansson, Phys. Rev. B **61**, 3131 (2000).
- ⁵⁹ Y. Yourdshahyan, U. Engberg, L. Bengtsson, B. I. Lundqvist, and B. Hammer, Phys. Rev. B **55**, 8721 (1997).
- ⁶⁰ Y. Yourdshahyan, C. Ruberto, L. Bengtsson, and B. I. Lundqvist, Phys. Rev. B **56**, 8553 (1997).
- ⁶¹ L. Smrcok, V. Langer, M. Halvarsson, and S. Ruppi, Zeitschrift fuer Kristallographie **216**, 409-412 (2001).
- ⁶² J. C. Boettger, Phys. Rev. B **55**, 750 (1997).
- ⁶³ F. C. Marton and R. E. Cohen, Am. Mineral. **79**, 789 (1994).
- ⁶⁴ H. d'Amour, D. Schiferl, W. Denner, H. Schulz, and W. B. Holzapfel, J. Appl. Phys. **49**, 4411 (1978).
- ⁶⁵ C. S. G. Cousins, J. Phys. C **14**, 1585-1602 (1981).
- ⁶⁶ J. Z. Sun, T. Stirner, and A. Matthews, Surf. Sci. **601**, 1358-1364 (2007).
- ⁶⁷ J. Lewis, D. Schwarzenbach, and H.D. Flack, Acta Crystallogr. A **38**, 733 (1982).
- ⁶⁸ J. D. McCullough and K. N. Trueblood, Acta Cryst. **12**, 507 (1959).
- ⁶⁹ G. Teufer, Acta Cryst. **15**, 1187 (1962).
- ⁷⁰ C. J. Howard, R. J. Hill, and B. E. Reichert, Acta Crystallogr., Sect. B: Struc. Sci. **44**, 116 (1988).

- ⁷¹ J.M. Léger, P.E. Tomaszewski, A. Atouf, and A. S. Pereira, Phys. Rev. B **47**, 14075 (1993) and references therein.
- ⁷² M. Fukuhara and I. Yamauchi, J. Mater. Sci. **28**, 4681 (1993).
- ⁷³ M. Fukuhara and A. Sampei, Phil. Mag. Lett. **80**, 325 (2000).
- ⁷⁴ P. Aldebert and J. P. Traverse, J. Am. Ceram. Soc. **68**, 34 (1985).
- ⁷⁵ H. M. Kandil, J. D. Greiner, and J. F. Smith, J. Am. Ceram. Soc. **67**, 341 (1984).
- ⁷⁶ R. P. Ingel and D. Lewis, J. Am. Ceram. Soc. **71**, 265 (1988).
- ⁷⁷ P. J. Botha, J. C. H. Chiang, J. D. Comins, P. M. Mjwara, and P. E. Ngoepe, J. Appl. Phys. **73**, 7268 (1993).
- ⁷⁸ J. C. Boettger, Phys. Rev. B **49**, 16798 (1994).
- ⁷⁹ J. Guo, D. E. Ellis, and D. J. Lam, Phys. Rev. B **45**, 13647 (1992).
- ⁸⁰ T. J. Godin and J. P. LaFemina, Phys. Rev. B **49**, 7691 (1994).
- ⁸¹ I. Batyrev, A. Alavi, and M. W. Finnis, Faraday Discuss. **114**, 33-43 (1999).
- ⁸² P. D. Tepesch and A. A. Quong, Phys. Stat. Sol. B **217**, 377 (2000).
- ⁸³ A. Marmier and M. W. Finnis, J. Phys.: Condens. Matter **14**, 7797 (2002).
- ⁸⁴ J. Z. Sun, T. Stirner, and A. Matthews, Surf. Coatings Technol. **201**, 4205 (2006).
- ⁸⁵ X.-G. Wang, A. Chaka, and M. Scheffler, Phys. Rev. Lett. **84**, 3650 (2000).
- ⁸⁶ C. Pascual and P. Duran, J. Am. Ceram. Soc. **66**, 22 (1983).
- ⁸⁷ R. Car and M. Parrinello, Phys. Rev. Lett. **55**, 2471 (1985).